Assessment of ADCIRC's Wetting and Drying Algorithm

J.C. Dietrich[a], R.L. Kolar[a], and R.A. Luettich[b]

[a]School of Civil Engineering and Environmental Science, University of Oklahoma,
Norman, OK, 73019, cdietrich@ou.edu, kolar@ou.edu

[b]Institute of Marine Sciences, University of North Carolina,
Morehead City, NC, 28557, rick_luettich@unc.edu

The ADvanced CIRCulation (ADCIRC) model is a finite-element hydrodynamic model based on the generalized wave continuity equation (GWCE). The model assumed fixed land boundaries until a wetting and drying algorithm was implemented by Luettich and Westerink in 1995 [1,2]. The algorithm uses an element-based approach, effectively turning elements on and off based on water depths and a water level gradient. While robust in some simulations, the algorithm can be subject to instabilities in the solution during highly nonlinear events. Thus, a rigorous assessment of the algorithm's stability, accuracy, mass balance properties, and parameter sensitivity under a variety of conditions is needed. Herein, we examine these issues using a one-dimensional implementation of the wetting and drying algorithm for basins with a linear slope; future studies will examine a wider variety of real and idealized basins. We believe the results of this work will benefit similar studies in two- or three-dimensions, for users and developers of both ADCIRC and other finite element models.

1. BACKGROUND

Shallow water equations are used by researchers and engineers to model the hydrodynamic behavior of oceans, coastal areas, estuaries, lakes and impoundments [3]. The finite element solutions of these equations have been improved by two equations: the wave continuity equation (WCE), introduced by Lynch and Gray [4] to suppress the spurious oscillations inherent to the primitive equations without having to dampen the solution either numerically or artificially; and the generalized wave continuity equation (GWCE), introduced by Kinnmark [5] to allow a balance between the primitive and pure wave forms of the shallow water equations by adding a weighted form of the primitive equation to the wave equation and using a weighting parameter *G*. The finite element model used in this paper, ADCIRC, was developed from the GWCE [6,7].

One area where ADCIRC and other hydrodynamic models may have problems is wetting and drying. Large-scale water behavior is often driven by wind and tides; for the latter, the most notable is the M_2 tide caused by the gravitational effects of the moon. Where the tides meet the shore, the water should move up and down the beach, causing areas to alternate between being wet and dry. Simply ignoring this behavior and treating the shoreline as a firm boundary, as was done in early versions of ADCIRC, allows the water to build up on boundary nodes as if against a

vertical wall, which also affects the manner in which waves reflect. Clearly, this can introduce phase and amplitude errors into near-shore circulation. A more physically-realistic model would turn on and off nodes and elements as the tide advances and recedes, as is done in recent versions of ADCIRC. However, many of its parameters have yet to be rigorously assessed, a problem which forms the basis for this study.

2. METHODS

In this section, we will discuss the implementation of a wetting and drying algorithm in the one-dimensional ADCIRC model. We will also describe our four model problems and the methods in which we assess the errors in our numerical results.

2.1. Wetting and Drying Algorithm

The one-dimensional ADCIRC wetting and drying algorithm is an approach developed by Luettich and Westerink [1,2] and is based on simplified physics and some empirical rules. The algorithm is located in the middle of the time loop, after the solution of the continuity equation but before the solution of the momentum equation. The algorithm is comprised of three parts.

First, the total water depth at every node is checked against a minimum wetness height, H_{min}. If the total water depth is larger than this minimum value, then the node remains active ("wet") and is included in the rest of the calculations. However, if the total water depth has fallen below this minimum value, then the node is deemed inactive ("dry") and removed from the calculations. Note that a dry node can have a positive water depth that is smaller than H_{min}. To help control oscillations, an input parameter allows the user to control the number of time steps that a node has to remain wet before it can be turned off; for all of the results in this paper, that parameter was set to 5 time steps.

Second, the steady state velocity that would result from a balance between the water level gradient and the bottom friction between a wet and an inactive node is checked against a minimum wetting velocity, U_{min}. The balance is given by:

$$U = \frac{g(\zeta_{i-1} - \zeta_i)}{\tau_i \Delta x_i}, \tag{1}$$

where g is gravity; ζ_{i-1} and ζ_i are the free surface elevations at the adjacent node and the node of interest, respectively; τ_i is the equivalent linear bottom friction coefficient (see Equation 7); and Δx_i is the grid spacing. Note that in many situations, only the free surface elevations will change significantly from time step to time step. In this case, the U_{min} criterion almost becomes a height restriction, where a node wets if the adjacent node's free surface elevation is sufficiently larger than its own. Again, to help control oscillations, another input parameter allows the user to control the number of time steps that a node has to remain inactive before it can be wetted; for all of the results in this paper, that parameter was set to 5 time steps.

Third, every landlocked wet node is tagged as inactive. A landlocked wet node is not connected to any active elements, and thus does not receive contributions to either side of the equation corresponding to that node. For some bathymetries, this criterion allows a node to remain inactive even if its total water depth is larger than the minimum wetting height. This is a slight change from the two-dimensional wetting and drying algorithm, which allows pockets of wet nodes to be surrounded by dry nodes. This allows wind stresses and other types of forcing to continue to act on the active elements. However, because we are not modeling wind stresses in this study, there is no reason to make landlocked nodes active.

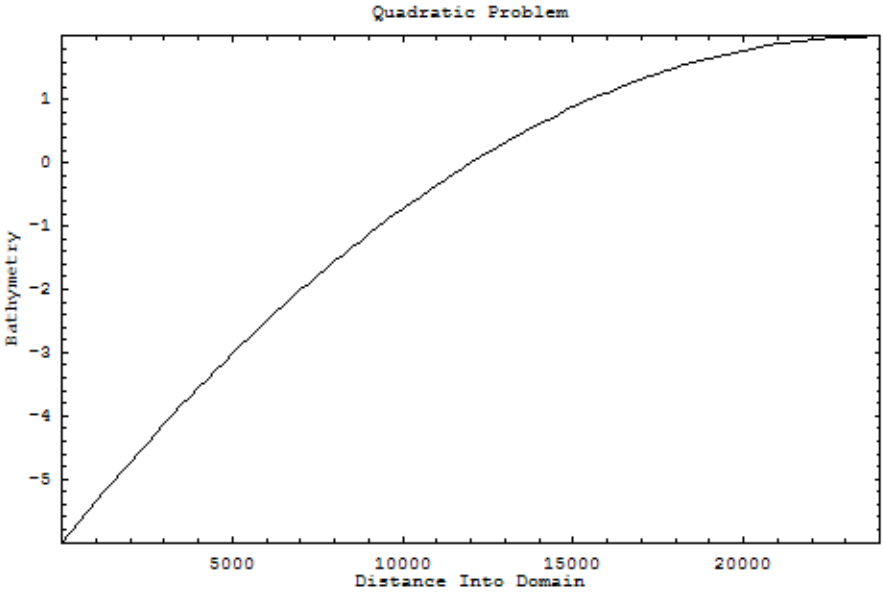

Figure 1. Bathymetry for the Quadratic Problem. Note that the bathymetric depth is 6 meters at the ocean boundary, the total length is 24 kilometers, and the undisturbed length is 12 kilometers.

2.2. Model Problems

The studies in this paper utilize four model problems with sloping beaches. These problems have open ocean boundaries on the left-hand side and are forced by a tidal amplitude.

The first model problem is similar to a test problem presented by Luettich and Westerink [1] in an earlier ADCIRC wetting-and-drying paper. We chose this bathymetry because: (1) it allows for a comparison with an analytical solution, as discussed in Section 3.1.1; and (2) it allows for a simple test case before moving forward to more complicated bathymetries. The problem has the following parameters (unless stated otherwise): a linear slope, an undisturbed length of 20 kilometers, a bathymetric depth at the open ocean boundary of 5 meters, a grid spacing of 250 meters, a time step of 10 seconds, a forcing amplitude of 0.25 meters, a tidal period of 12 hours (43,200 seconds), a duration of 4 tidal periods, a *cftau* value of 0.001 and a *G* value of 0.001 sec^{-1} (both defined in Section 3.1.3), an H_{min} value of 0.01 meters, and a U_{min} value of 0.01 meters per second. We will refer to this as Linear Problem 1.

The second model problem creates a situation where waves can wet and dry a larger number of nodes on the beach. This problem is deeper but shorter, and it allows wave run-up to cover more of the beach. This problem has the following parameters (unless stated otherwise): a linear slope, an undisturbed length of 18 kilometers, a bathymetric depth at the open ocean boundary of 6 meters, a grid spacing of 250 meters, a time step of 10 seconds, a forcing amplitude of 1.0 meter, a tidal period of 12 hours (43,200 sec), a duration of 4 tidal periods, a *cftau* value of 0.001 and a *G* value of 0.001 sec^{-1} (both defined in Section 3.1.3), an H_{min} value of 0.01 meters, and a U_{min} value of 0.01 meters per second. We will refer to this as Linear Problem 2.

The third model problem uses a quadratic sloping beach, as shown in Figure 1. This problem has the following parameters (unless stated otherwise): a quadratic slope, an undisturbed length of 12 kilometers, a bathymetric depth at the open ocean boundary of 6 meters, a grid

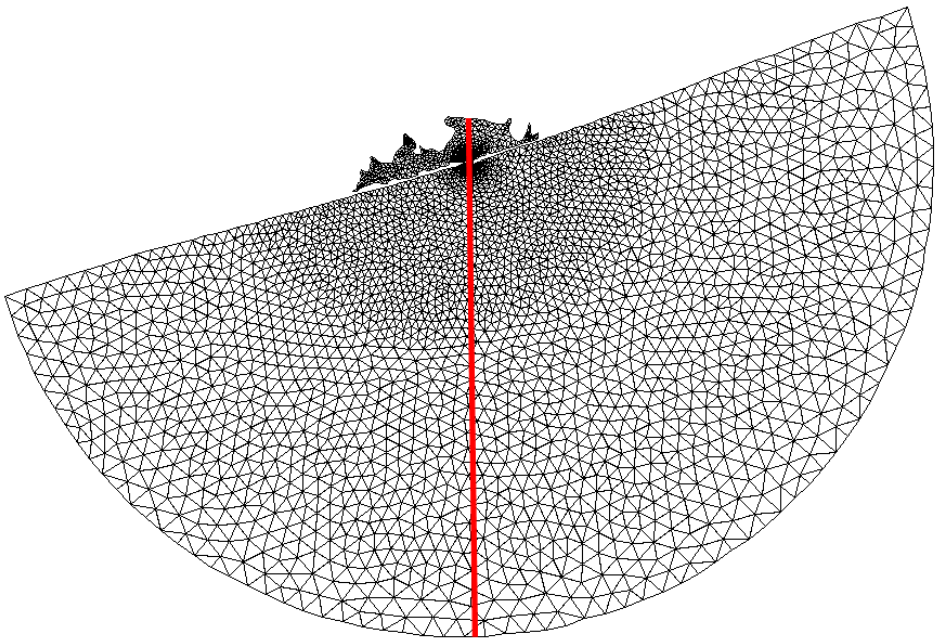

Figure 2. The finite element grid for the two-dimensional Beaufort Inlet domain. Note that the resolution is high around the inlet itself, but that it decreases near the ocean boundary. A schematic of the one-dimensional slice used in this study is shown in red. It begins inside the inlet, moves through the opening, and ends at the open ocean boundary.

spacing of 250 meters, a time step of 10 seconds, a forcing amplitude of 1.0 meter, a tidal period of 12 hours (43,200 sec), a duration of 4 tidal periods, a *cftau* value of 0.001 and a G value of 0.001 sec^{-1} (both defined in Section 3.1.3), an H_{min} value of 0.01 meters, and a U_{min} value of 0.01 meters per second. We will refer to this as the Quadratic Problem.

The fourth model problem is a one-dimensional slice of a two-dimensional domain. The finite element grid for the Beaufort Inlet domain is shown in Figure 2. Beaufort Inlet is located on the coast of North Carolina, and has been used to model larvae transport and hurricane storm surges in the barrier island region [14]. The grid in Figure 2 is a "first-generation" domain, in that it does not include the more complex geometry and bathymetry typical of Beaufort Inlet. However, its realistic bathymetry is still an appropriate test of the wetting and drying algorithm, especially in one-dimension. We extracted a one-dimensional slice from this domain. The slice runs approximately north-to-south, beginning within the inlet and ending at the open ocean boundary, as shown in Figure 2. The bathymetry for this slice is shown in Figure 3. Note that this problem is significantly deeper than the idealistic model problems, and the bathymetry is much more varied, especially near the inlet itself. Also note that, because we followed the resolution in the two-dimensional domain, this one-dimensional domain utilizes a variable grid spacing. This problem has the following parameters (unless stated otherwise): an undisturbed length of 56.8 kilometers, a bathymetric depth at the open ocean boundary of about 53 meters, a variable grid spacing, a time step of 10 seconds, a forcing amplitude of 1.0 meter, a tidal period of 12 hours (43,200 sec), a duration of 4 tidal periods, a *cftau* value of 0.001 and a G value of 0.001 sec^{-1} (both defined in

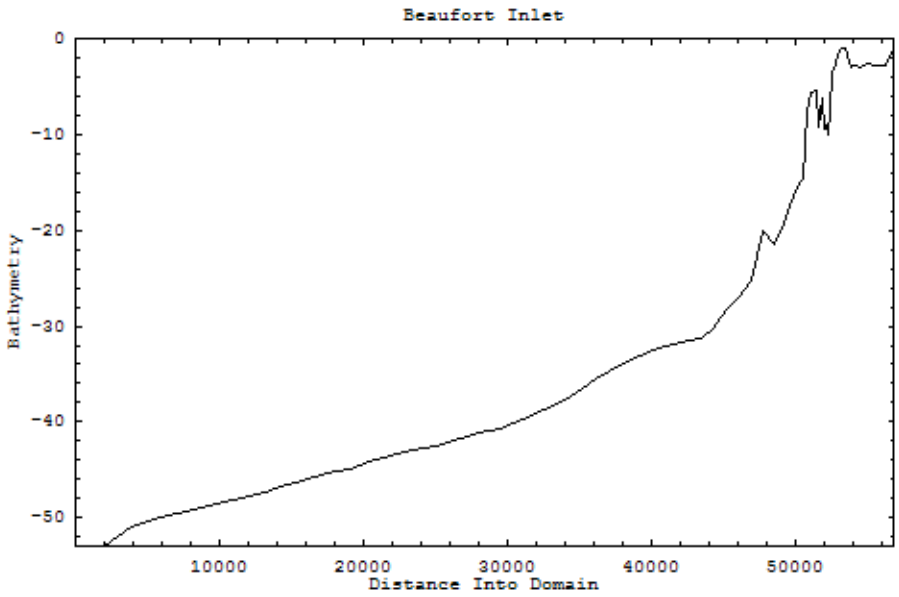

Figure 3. Bathymetry for the Inlet Problem. The opening between the inlet and the ocean is located about 51 kilometers into the domain, where the depth is about 10 meters. Note that the bathymetric depth ranges from a maximum of about 53 meters at the ocean boundary, to 0.94 meters at a distance of 53 kilometers into the domain. The total length of the domain is 56.8 kilometers.

Section 3.1.3), an H_{min} value of 0.01 meters, and a U_{min} value of 0.01 meters per second. We will refer to this as the Inlet Problem.

2.3. Error Computations

Our sensitivity studies utilize a comparison between our numerical results and the analytical solution described in Section 3.1.1. This comparison is calculated through an examination of the position of the wet/dry interface over the fourth tidal period (because the model is spun up from a cold start for the first three periods). After every 10 minute interval in that fourth period, we calculate the difference between the position of the interface given by the numerical results and the position of the interface given by the analytical solution. These differences are then averaged. If the numerical results successfully approximate the analytical solution, then the average difference should be zero. However, spatial discretization often prevents a perfect match between numerical and analytical, so we are satisfied if the average difference is less than the grid spacing of 250 meters.

Our studies also utilize a computation of mass balance error. This is a cumulative mass balance error over the entire simulation. It is calculated using a finite volume approach, where we compute the difference between the global accumulation and the global mass flux, as represented by the primitive continuity equation. Recently, several papers [8,9] have advocated computing mass balance from finite element residuals in order to be consistent with the numerical discretization. However, we have shown (Kolar et al. [13]) the finite volume approach to be a good surrogate variable for accuracy and phasing errors; that is, small mass balance errors (as computed with finite volume) correlate with small constituent errors. Hence our reason for using the finite volume approach herein.

3. NUMERICAL EXPERIMENTS

In this section, we discuss the results of several tests involving the wetting and drying algorithm and our model problems. We will first examine two versions of the linear-sloping beach, then the quadratic-sloping beach, and then the slice of Beaufort Inlet.

3.1. Linear Problems

The results in this subsection are from tests on the two model problems with linear-sloping beaches. First, we compare the numerical results with an analytical solution. Second, we examine the algorithm's effect on temporal stability. Third, we conduct parameter sensitivity studies for bottom friction and the G numerical parameter. Fourth, we conduct parameter sensitivity studies for the wetting and drying parameters H_{min} and U_{min}. Fifth, we examine the effect of spatial resolution on the performance of the algorithm.

3.1.1. Comparison with an Analytical Solution

The classic analytical solution for wave run-up on a sloping beach was first expressed by Carrier and Greenspan [10] and later revisited by Johns [11] and Siden and Lynch [12]. The solution is quite restrictive; it describes the behavior of a frictionless wave on a linearly-sloped beach. The one-dimensional wetting-and-drying ADCIRC model incorporates bottom friction and can be applied to complex bathymetries. However, it is important to verify its performance against an analytical solution in this simple test case.

The full equations for the analytic solution are given in the latter two references. We will reproduce the important ones here. The equations for the velocity, horizontal position, and elevation of the shoreline are given by:

$$u = \frac{\partial \xi}{\partial t} = -u\frac{\partial u}{\partial t} - \frac{2A\pi}{T}\left(1 + \frac{\partial u}{\partial t}\right)\sin\left(\frac{2\pi}{T}(t+u)\right), \tag{2}$$

$$\xi = -\frac{1}{2}u^2 + A\cos\left(\frac{2\pi}{T}(t+u)\right), \tag{3}$$

and

$$\zeta = \xi, \tag{4}$$

where u is the scaled velocity, ξ is the scaled horizontal displacement, A is the scaled amplitude, T is the scaled period, t is the scaled time, and ζ is the scaled free surface elevation from the mean. Note that Equation 4 holds true because the scaling changes the slope to 45 degrees. We solve for u in Equation 2 by using an iterative technique, a finite difference approximation on the $\partial u / \partial t$ terms, and the knowledge that the velocity of the shoreline at maximum inundation is zero. Once the shoreline information is calculated, then the velocity and elevation at interior points can be calculated using the following equations:

$$u = -\frac{4AJ_1\left(\frac{4\pi\sqrt{\zeta - x}}{T}\right)}{\alpha}\sin\left(\frac{2\pi}{T}(t+u)\right), \tag{5}$$

and

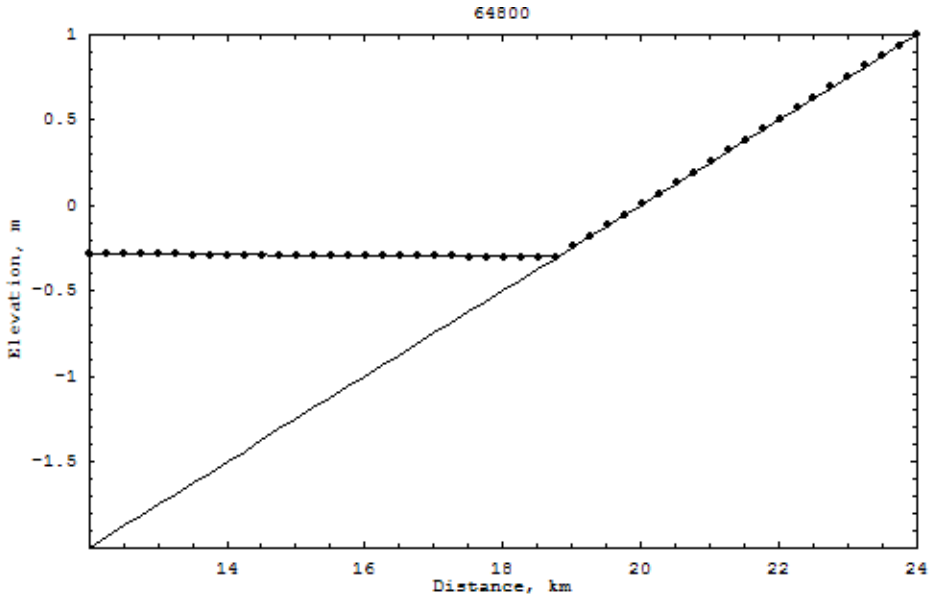

Figure 4. The numerical results (black dots) and the analytical solution (solid line) halfway through the second tidal cycle. The solid diagonal line is the bathymetry. Note that the number at the top of the figure is the time in seconds.

$$\zeta = -\frac{1}{2}u^2 + AJ_0\left(\frac{4\pi\sqrt{\zeta - x}}{T}\right)\cos\left(\frac{2\pi}{T}(t+u)\right), \tag{6}$$

where J_0 and J_1 are Bessel functions and x is scaled horizontal position. Equation 5 and Equation 6 must also be solved iteratively. Note that the ADCIRC boundary forcing was adjusted to match the cosine forcing of the analytical solution.

We attempted to match our numerical results with the analytical solution by using Linear Problem 1. Figure 4 and Figure 5 show the analytical solution and numerical results at two different times in the second tidal cycle. (Without a ramp function to smooth the transition from a cold start, the numerical solution experiences some start-up noise during the first tidal cycle.) Note that the numerical results show good agreement with the analytical solution and that there is no friction-induced lag at the shoreline. We believe the good agreement is due to our relatively small value of *cftau*, so that the bottom friction does not dominate the momentum balance. Note that ADCIRC is not stable with a bottom friction coefficient of zero, so an exact comparison to the analytical solution is impossible.

Figure 6 shows the position of the shoreline over the first three tidal periods. (This is similar to Figures 2 and 3 in Johns [11].) After the numerical results fight through the noise of the first tidal period, they show very good agreement with the analytical solution. There is some visible lag during the wetting phase, which raises the question of whether we need to relax our wetting criterion. That question will be addressed in a parameter study in Section 3.1.4; for now, we believe the information in these figures shows that the ADCIRC model can provide accurate results for this simple test case.

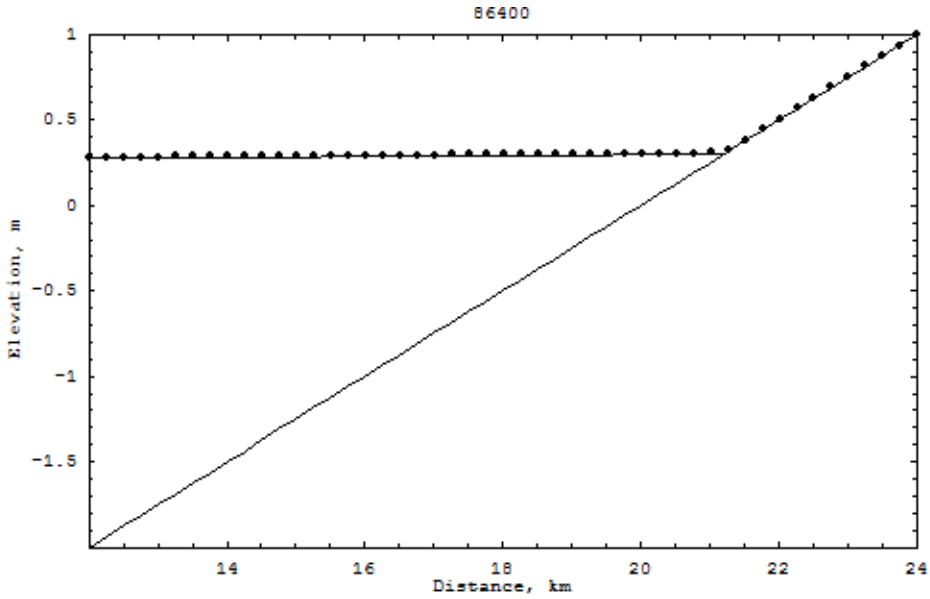

Figure 5. The numerical results (black dots) and the analytical solution (solid line) at the end of the second tidal cycle. The solid diagonal line is the bathymetry. Note that the number at the top of the figure is the time in seconds.

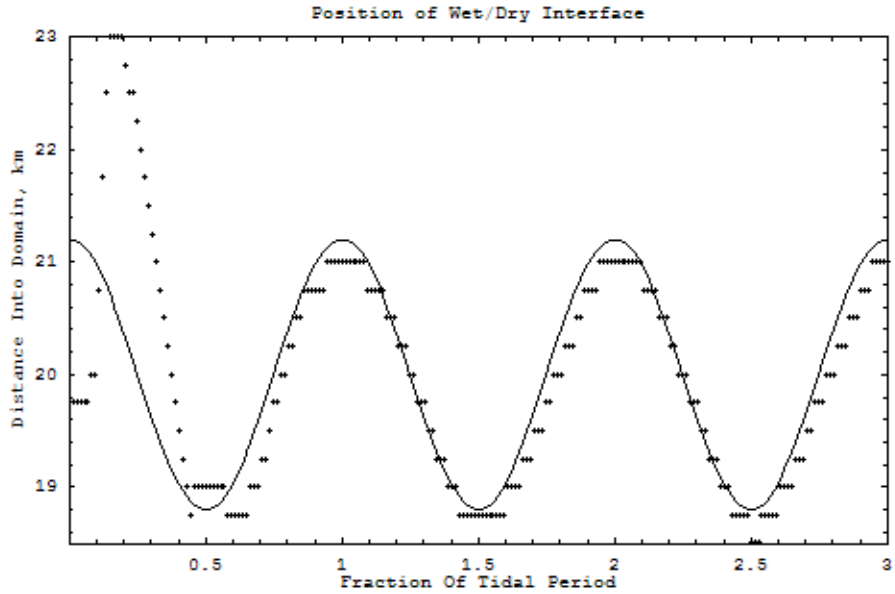

Figure 6. The position of the shoreline, as given by the numerical results (black dots) and the analytical solution (solid line) for the first three tidal periods.

3.1.2. Hueristic Stability

Stability was measured by determining the maximum time step (within 5 seconds) at which the model still provided valid results. However, it is difficult to measure the impact of the wetting and drying algorithm on stability because our model problems cannot be run with the original fixed-boundary ADCIRC model. In order to prevent instabilities during the ebb phase when nodes should dry but cannot, we altered our model problems so that they could be run with the original model.

For Linear Problem 1, we shortened the domain to 16 kilometers so that there is a bathymetry of 1 meter at the land boundary. This prevents the 0.25 meter forcing amplitude from trying to dry out nodes on the beach. All of the other parameters, including the slope, remained the same. Under these conditions, the original ADCIRC model provided a maximum stable time step of 60 seconds. The wetting and drying model, when applied to the unaltered Linear Problem 1, provided a maximum stable time step of 55 seconds. This is a decrease of 8.3 percent.

For Linear Problem 2, we shortened the domain to 12 kilometers so that there is a bathymetry of 2 meters at the land boundary. This prevents the 1 meter forcing amplitude from trying to dry out nodes on the beach. All of the other parameters, including the slope, remained the same. The original ADCIRC model provided a maximum stable time step of 50 seconds. The wetting and drying model, when applied to the unaltered Linear Problem 2, provided a maximum stable time step of 15 seconds. This is a decrease of 70 percent.

Note that, for both problems, mass balance errors were an order of magnitude greater for the wetting and drying model. These errors were concentrated on the beach where nodes are turned on and off.

3.1.3. Parameter Sensitivity - *cftau* and *G*

Two important parameters in the ADCIRC model are *cftau* and *G*, the former being a physical parameter and the latter being purely numerical. The parameter *cftau* controls bottom friction in the model. It is used as a coefficient in the calculation of the equivalent linear bottom friction coefficient, τ, in the momentum equation for each node *i*:

$$\tau_i = cftau\left(\frac{|u_i|}{H_i}\right). \tag{7}$$

Note that the magnitude of τ is directly proportional to the magnitude of *cftau*; as *cftau* goes to zero, so does *tau*. As expected, bottom friction plays a significant role in the wetting and drying process. Its relative magnitude increases in shallower, near-shore waters and hence it directly affects the speed at which waves inundate or recede.

The parameter *G* is the numerical parameter introduced by Kinnmark [5] to control the balance between the wave continuity equation and the primitive continuity equation. As *G* is decreased, the GWCE become more like a pure wave equation; as *G* is increased, the GWCE more closely approximates the primitive equation. As reported elsewhere [13], if *G* is too high, the solution develops spurious oscillations, which prevent the model from capturing the behavior of the waves.

Because these two parameters are related in their effects on the model's behavior, it is important to examine them in tandem. Kolar et al [13] determined an optimal range of G/τ to be on the order of 1 to 10. However, that study examined the effects of these parameters on barotropic tides without wetting and drying. Herein, we examine their effects on wetting and drying by varying the parameters *cftau* and *G* from 0.000001 to 0.5 (always in sec^{-1} for *G*; *cftau* is dimen-

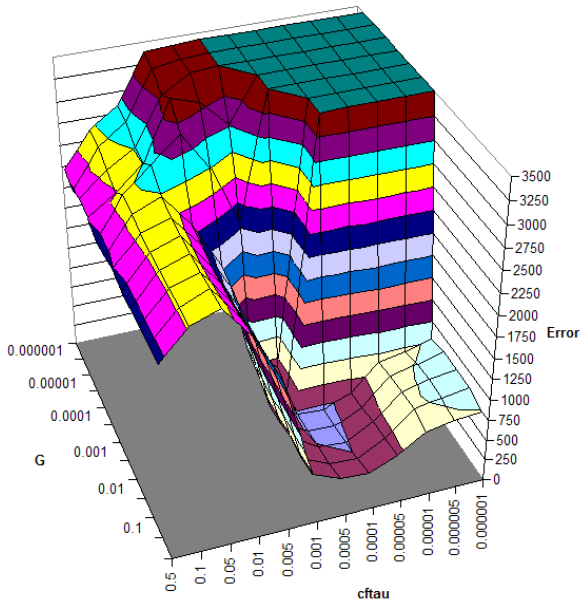

Figure 7. The average difference between the numerical results and the analytical solution over the fourth tidal cycle, as discussed in Section 2.3, for 144 combinations of *cftau* and *G*. The errors are shown in intervals of 250 meters, which is the grid spacing.

sionless), creating a matrix of *cftau*-*G* combinations. For each combination, we compared the behavior of the model with the analytical solution described above, and we examined the model's mass balance properties. The tests in this section use Linear Problem 2.

The comparison with the analytical solution was performed by averaging the differences between the numerical results and the analytical solution over the fourth tidal cycle, as discussed above in Section 2.3. By plotting these averages for each combination in the matrix, we developed a three-dimensional surface that is shown in Figure 7. However, we can share some observations from this surface. First, the model is unstable in almost one fourth of the matrix, in the region where both *cftau* and *G* approach 0.000001. It is stable, however, in the regions where only one of these parameters approaches this minimum value. Second, the model is significantly more sensitive to variations in *cftau*. The variations with regard to *G* are not nearly so pronounced.

Third, in general, the average differences between the numerical results and the analytical solution decrease as *cftau* is decreased. This trend is intuitive, considering the analytical solution is frictionless. A slice of the matrix where *cftau* is held constant at a value of 0.000001 and *G* is varied would show average differences on the magnitude of three times the grid spacing of 250 meters.

Interestingly, the best agreement between the numerical results and the analytical solution occurs with a combination such as *cftau* = 0.0001 and $G = 0.01$ sec^{-1}, which provides an average difference of 211 meters, or less than one grid spacing. Figure 8 shows the position of the wet/dry interface over time for a simulation using this combination. The numerical results experience some start-up noise during the first two tidal cycles, but then they show very good agreement with the analytical solution during the fourth tidal cycle. We will use this combination of *cftau* and *G*

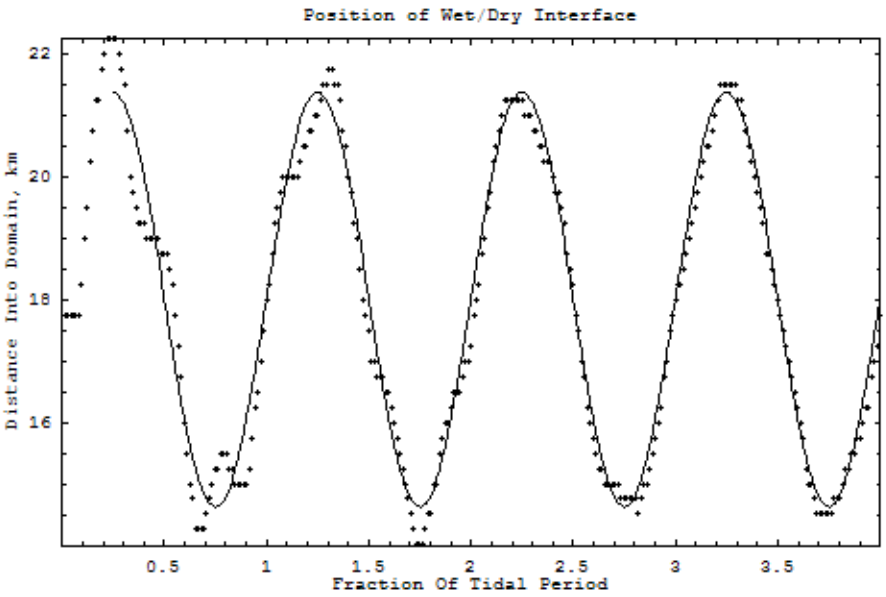

Figure 8. The position of the shoreline, as given by the numerical results (black dots) and the analytical solution (solid line) for the first four tidal periods.

in Section 3.1.4, where we are explicitly trying to match the analytical solution. However, it should be remembered that the analytical solution does not include bottom friction, so it will not be accurate for all situations. In general, the values of *cftau* and *G* should be determined based on the bottom friction requirements of the particular simulation.

The examination of the model's mass balance properties was performed in the same manner, by creating a matrix of *cftau*-*G* combinations. The mass balance error was calculated using the finite volume approach, described in Section 2.3. Using these average mass balance errors, we created another three-dimensional surface, this time shown in Figure 9. The model is unstable for the same region of combinations, where both *cftau* and *G* approach 0.000001. However, if *G* remains relatively large, then *cftau* can be decreased without significant penalty. For example, a typical range of cftau from 10^{-3} to 10^{-5} shows: (1) mass balance errors on the order of 2,000 square meters, or approximately 3.7 percent of the total undisturbed water area; and (2) when *G* is decreased to its minimum stable value, ratios of G/τ are in the range of 1 to 10 (optimum range reported by Kolar et al. [13] in their fixed-boundary barotropic studies). Note that values of cftau larger than 10^{-3} do show good mass balance, but they produce unrealistically damped simulations.

3.1.4. Parameter Sensitivity - H_{min} and U_{min}

Another pair of important numerical parameters is H_{min} and U_{min}, described above in Section 2.1. Both parameters affect the ability of the algorithm to wet or dry nodes. The parameter H_{min} controls the drying phase, and the parameter U_{min} controls the wetting phase. For example, a large value for H_{min} would allow nodes to dry while still holding a significant amount of water, causing nodes to dry much faster than they should. Similar problems would be experienced if the value for H_{min} is too small or if the value of U_{min} is at either extreme. Thus, it is important to consider the effects of the two parameters in tandem.

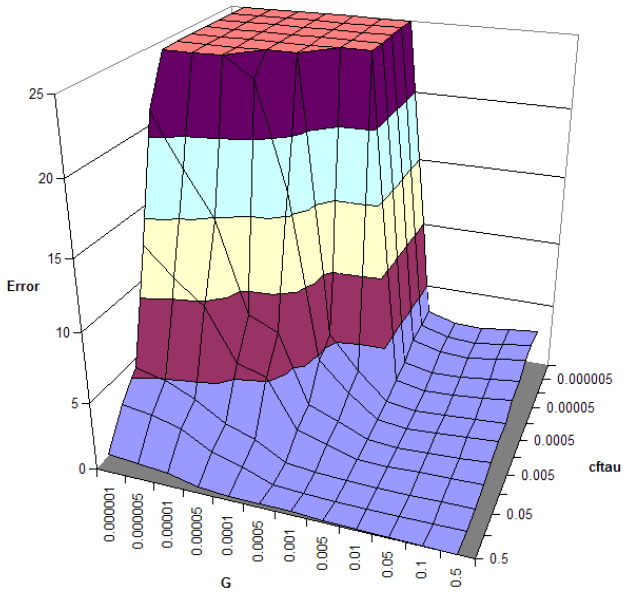

Figure 9. Mass balance errors for 144 combinations of *cftau* and *G*. The errors are shown in intervals of 5,000 square meters. The errors in the region at the front of the graph are on the order of 1,000 to 2,000 square meters, or 1.9 to 3.7 percent of the undisturbed water area.

We accomplished this consideration by using the same technique as for *cftau* and *G*. We examined the effects of H_{min} and U_{min} by varying each parameter from 0.0001 to 0.5 (meters for H_{min}; meters per second for U_{min}), creating a matrix of H_{min}-U_{min} combinations. For these runs, we used *cftau* = 0.0001 and $G = 0.01$ sec^{-1}, which the previous study found to produce meaningful solutions. We also used Linear Problem 2. For each combination of H_{min} and U_{min}, we compared the behavior of the model with the analytical solution and we examined the model's mass balance properties.

The comparison with the analytical solution was performed by using the same technique as above, where we built a matrix of average differences between the numerical results and the analytical solution, as shown in Figure 10. We offer the following observations. First, the model does not go unstable anywhere in the range from 0.0001 to 0.5. In fact, we were able to successfully decrease H_{min} to 10^{-10} meters; the model behaves similarly for all values of H_{min} less than 0.01 meters. However, increasing H_{min} beyond the upper limit of this range does cause instabilities, especially for unrealistic values such as 10 meters. Second, the parameter U_{min} has no significant effect on the behavior of the model for the conditions of this problem. In this graph, there is no noticeable change between the average differences for the extreme values of U_{min} = 0.0001 meters per second and U_{min} = 0.5 meters per second. Results are insensitive to the parameter U_{min} for this test problem.

The examination of the model's mass balance properties was performed in the same manner as described in Section 2.3. The mass balance error was calculated by computing the difference between the global accumulation and the global mass flux. A three-dimensional surface of average mass balance errors over four tidal cycles is shown in Figure 11, and it reveals the following. First, again, the model does not experience instabilities for any combination of H_{min} and

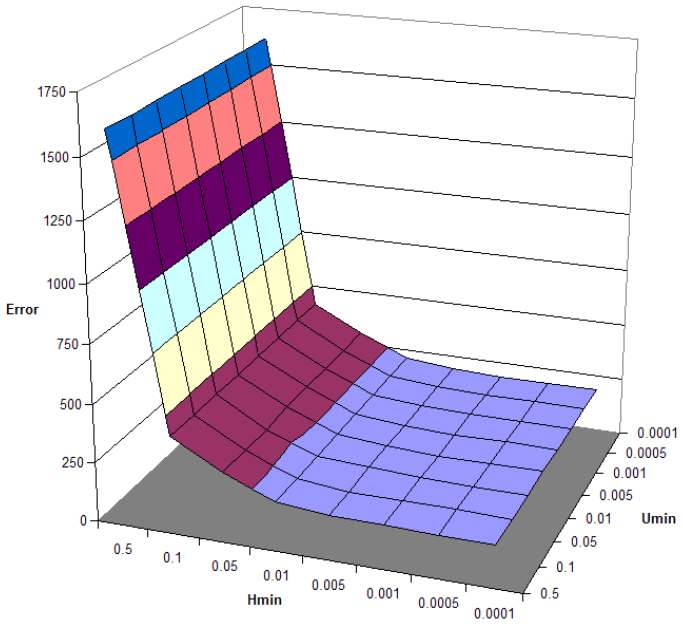

Figure 10. The average difference between the numerical results and the analytical solution in their calculation of the position of the shoreline over the fourth tidal cycle. (See Section 2.3.) The error is shown in intervals of 250 meters, which is the grid spacing.

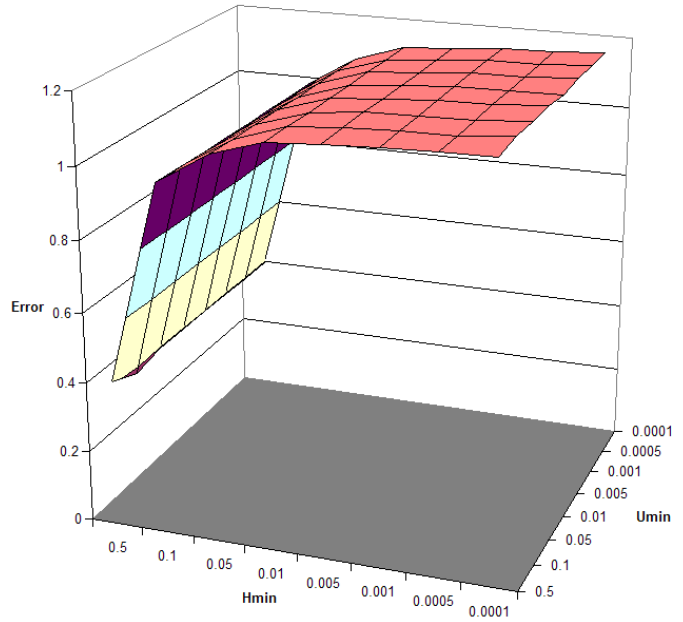

Figure 11. The mass balance errors for a range of H_{min} and U_{min} values. (See Section 2.3.) The errors are shown in intervals of 200 square meters.

U_{min} within the range from 0.0001 to 0.5. Second, the wetting criterion U_{min} does not have an effect on mass balance. Third, the average mass balance errors decrease as H_{min} is increased.

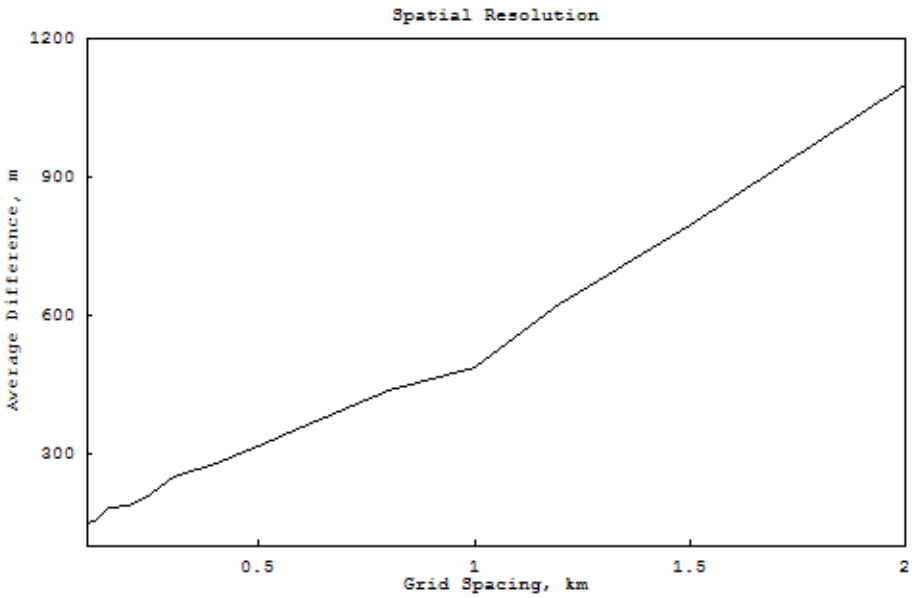

Figure 12. The average difference between the numerical results and the analytical solution. (See Section 2.3.)

The errors decrease from a steady 1100 square meters when H_{min} is less than 0.01 to about 400 square meters when H_{min} = 0.5. However, this decrease is at the expense of accuracy, as discussed above and shown in Figure 10. For such a large value of H_{min}, the numerical results are unable to match the analytical solution.

Thus, results indicate an optimal value for these two parameters H_{min} and U_{min} is around 0.01. There does not appear to be a lower limit for either parameter; however, nothing is gained by decreasing either parameter to the limits of machine precision. We will continue to use values of 0.01 for both parameters.

3.1.5. Spatial Resolution

Spatial resolution also plays a significant role in the simulation of wetting and drying, because it controls the model's ability to follow the position of the shoreline as it inundates and recedes. Using Linear Problem 2, we varied the spatial resolution from a minimum of 100 meters to a maximum of 2000 meters. For each grid spacing, we compared the behavior of the model with the analytical solution and we examined the model's mass balance properties.

Figure 12 shows the average difference between the numerical results and the analytical solution for the various spatial resolutions. Note that all of the simulations were run with a time step of 10 seconds except for those with spatial resolutions of 100 meters and 120 meters, which were run with a time step of 1 second in order to maintain stability. The graph shows a sublinear (0.64) convergence rate as the grid spacing is decreased.

Figure 13 shows the mass balance errors for the various spatial resolutions. This graph supports the use of the finite volume approach as a predictor of model behavior because, as the grid spacing is decreased, the mass balance errors also decrease.

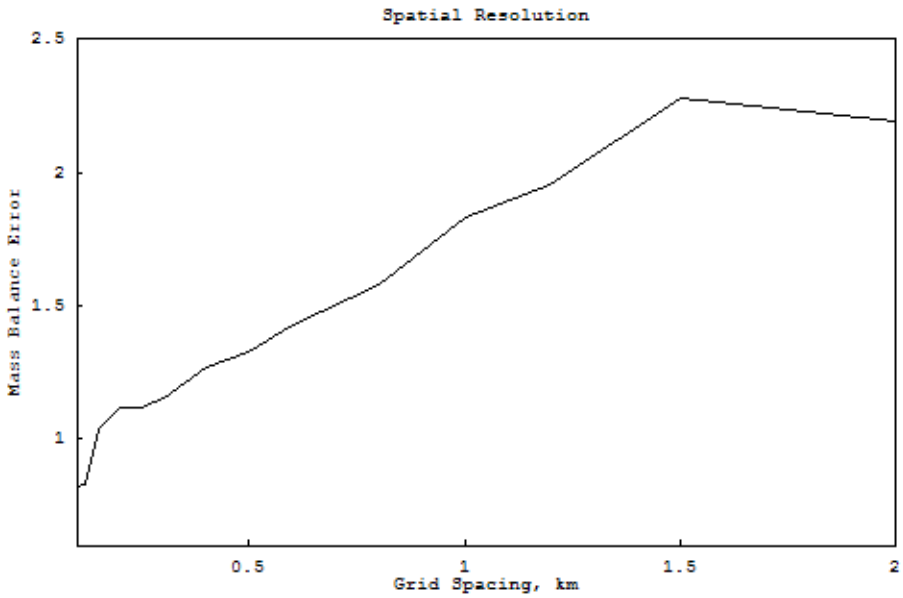

Figure 13. Mass balance errors (10^3 square meters) for a range of spatial resolutions. (See Section 2.3.)

3.2. Quadratic Problem

The results in this subsection are from tests on a model problem with a quadratic-sloping beach. First, we examine the algorithm's effect on temporal stability. Second, we conduct parameter sensitivity studies for bottom friction and the G numerical parameter. Third, we conduct parameter sensitivity studies for the wetting and drying parameters H_{min} and U_{min}. Fourth, we examine the effect of spatial resolution on the performance of the algorithm.

3.2.1. Hueristic Stability

Stability was measured by determining the maximum time step (within 5 seconds) at which the model still provided valid results. However, we encountered the same problem that we had with the sloping beach, viz, our wetting and drying model problems cannot be run with the original fixed-boundary ADCIRC model. In order to prevent instabilities during the ebb phase when nodes should dry but cannot, we altered our model problem so that it can be run with the original model.

For the Quadratic Problem, we shortened the domain to 7 kilometers so that there is a bathymetry of 2 meters at the land boundary. This prevents the 1 meter forcing amplitude from trying to dry out nodes on the beach. All of the other parameters, including the slope, remained the same. The original ADCIRC model provided a maximum stable time step of 45 seconds. The wetting and drying model, when applied to the unaltered Quadratic Problem, provided a maximum stable time step of 15 seconds, which is a decrease of 66 percent.

Note that, once again, the wetting and drying problem experienced larger local mass balance errors, and they were concentrated on the beach where nodes are turned on and off.

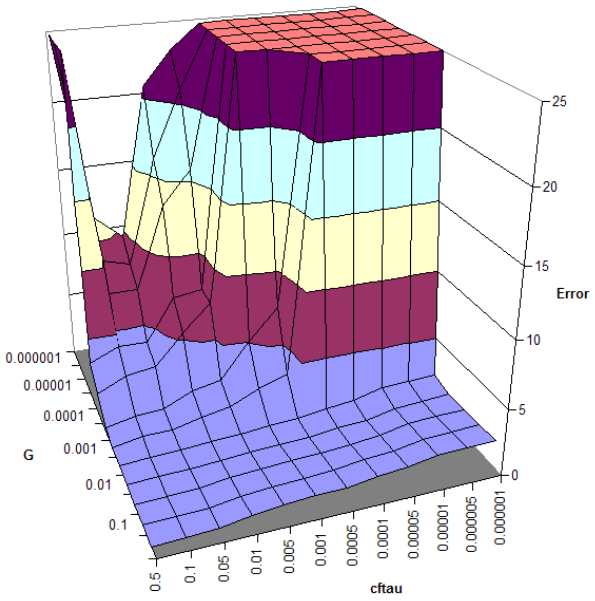

Figure 14. Mass balance errors for 144 combinations of *cftau* and *G*. The errors on the vertical axis are shown in intervals of 5,000 square meters. The errors in the region where *cftau* and *G* are near maximum are 500 square meters or less.

3.2.2. Parameter Sensitivity - *cftau* and *G*

The effects of the ADCIRC model parameters *cftau* and *G* on the wetting and drying algorithm were again examined. As described above in Section 3.1.3, the parameter *cftau* controls the bottom friction in the model, and the parameter *G* controls the balance between the wave continuity equation and the primitive continuity equation. Herein, we examine their effects on wetting and drying by varying the parameters from 0.000001 to 0.5 (always in sec^{-1} for *G*; *cftau* is dimensionless), creating a matrix of *cftau*-*G* combinations. For each combination, we examined the model's mass balance properties. Note that we were unable to compare the behavior of the model with an analytical solution, because such a solution does not exist for a quadratic sloping beach. Also note that previous work has shown that mass balance errors, as computed with a finite volume approach, correlate well with truncation errors.

The average mass balance error for each combination is shown as a surface plot in Figure 14. The mass balance error was calculated using the finite volume approach, which is described in Section 2.3. We offer several observations. First, the model is unstable for the same region of *cftau*-*G* combinations as it was for the linear sloping beach, namely when both parameters are decreased below 0.001. Second, the shape of the three-dimensional surface is similar to the shape of the surface for the linear sloping beach in Figure 9. The only exception is a spike in this graph at the combination of *cftau* = 0.5 and *G* = 0.000001. However, although the shapes of the two graphs are similar, the magnitude of the mass balance errors are slightly smaller for the quadratic sloping beach. The errors in the region where *cftau* and *G* are near maximum are on the order of 500 square meters, or approximately 1.5 percent of the undisturbed water area. And some errors are even less; the minimum occurs at the combination of *cftau* = 0.5 and *G* = 0.05, where the aver-

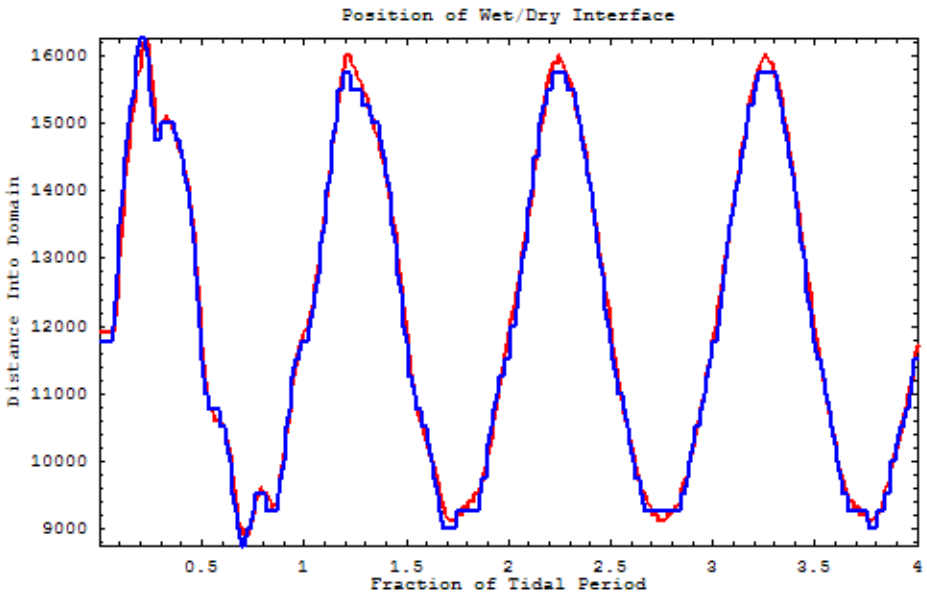

Figure 15. The position of the shoreline for the combination of *cftau* = 0.0001 and $G = 0.01$. The blue line is a coarse solution ($\Delta x = 250$ meters, $\Delta t = 10$ seconds), and the red line is a fine solution ($\Delta x = 100$ meters, $\Delta t = 1$ second).

age mass balance error is 16.3 square meters, or approximately 0.05 percent of the undisturbed water area. The corresponding error for the linear sloping beach was 41.1 square meters, or 0.07 percent of the undisturbed water area. Overall, as the values of *cftau* and G increase, the model's mass balance properties improve.

We were unable to quantitatively assess (a la Figure 7) the algorithm's impact on accuracy because we do not have an analytical solution for a quadratic sloping beach. However, we believe the behavior is similar to that observed for the linear sloping beach; large values for *cftau* prevent the wetting and drying algorithm from capturing the behavior of the shoreline. Figures 15 and 16 show the position of the shoreline for different resolutions and combinations of *cftau* and G. In Figure 15, we show the combination of *cftau* = 0.0001 and $G = 0.01$, which was in the region of optimal accuracy for the linear sloping beach. Note that the normal coarse solution (blue line) of $\Delta x = 250$ meters and $\Delta t = 10$ seconds provides a reasonably close match to the fine solution (red line) of $\Delta x = 100$ meters and $\Delta t = 1$ second. However, if we increase the value of *cftau*, as in Figure 16, we do not achieve nearly as good of a match. The coarse solution recedes 700 meters farther down the shoreline than does the fine solution, and there is a lag in the drying phase. In addition, when compared with Figure 15, the range of inundation and recession is considerably smaller. The maximum inundation is down from 16.2 kilometers to 15.2 kilometers, and the maximum recession is up from 8.75 kilometers to 10.0 kilometers. The larger value of *cftau* prevents the algorithm from wetting and drying as much of the beach, because, as *cftau* increases, so does the bottom friction. Thus, although we cannot quantitatively assess the impact of these parameters on the accuracy of the algorithm, our qualitative analysis suggests that they behave similarly for quadratic sloping and linear sloping beaches.

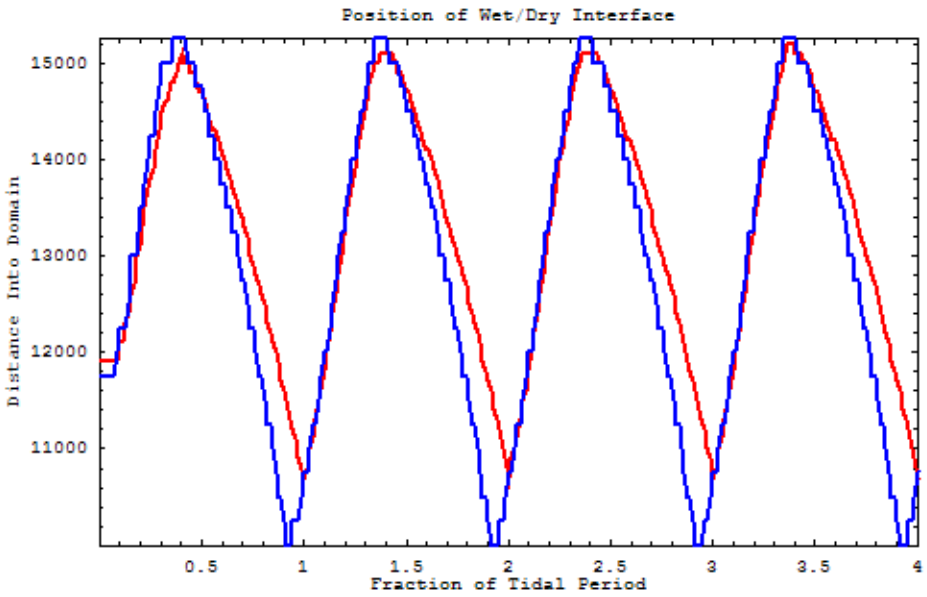

Figure 16. The position of the shoreline for the combination of *cftau* = 0.01 and $G = 0.01$. The blue line is a coarse solution ($\Delta x = 250$ meters, $\Delta t = 10$ seconds), and the red line is a fine solution ($\Delta x = 100$ meters, $\Delta t = 1$ second).

3.2.3. Parameter Sensitivity - H_{min} and U_{min}

Another pair of numerical parameters is H_{min} and U_{min}, described above in Section 2.1 and Section 3.1.4. Both parameters affect the ability of the algorithm to wet or dry nodes, so it is important to consider the effects of the two parameters in tandem.

We accomplished this by varying each parameter from 0.0001 to 0.5 (meters for H_{min}; meters per second for U_{min}), creating a matrix of combinations. For these runs, we again used *cftau* = 0.0001 and $G = 0.01$ sec^{-1}, partially to match the study in Section 3.1.4 and partially because we believe this is an accurate combination, based on the results in Section 3.1.3 and Section 3.2.2. For each combination of H_{min} and U_{min}, we examined the model's mass balance properties.

The examination of the model's mass balance properties was performed in the same manner as described in Section 2.3. The mass balance error was calculated by computing the difference between the global accumulation and the global mass flux. A three-dimensional surface of average mass balance error over four tidal cycles is shown in Figure 17, and it reveals the following. First, the model does not experience instabilities for any combination of H_{min} and U_{min} within the range from 0.0001 to 0.5. Second, as with the linear sloping problem, the wetting criterion U_{min} does not have an effect on mass balance for the quadratic sloping beach. There is not a significant difference between the average mass balance errors for the extreme values of U_{min} = 0.0001 meters per second and U_{min} = 0.5 meters per second. Third, the average mass balance errors decrease as H_{min} is increased. The errors decrease from a steady 900 square meters when H_{min} is less than 0.01 meters to about 250 square meters when H_{min} = 0.5 meters. Fourth, as with the *cftau*-*G* test, the average mass balance errors are slightly smaller for the quadratic sloping beach than they are for the linear sloping beach. The plateau of 900 square meters in Figure 17 is

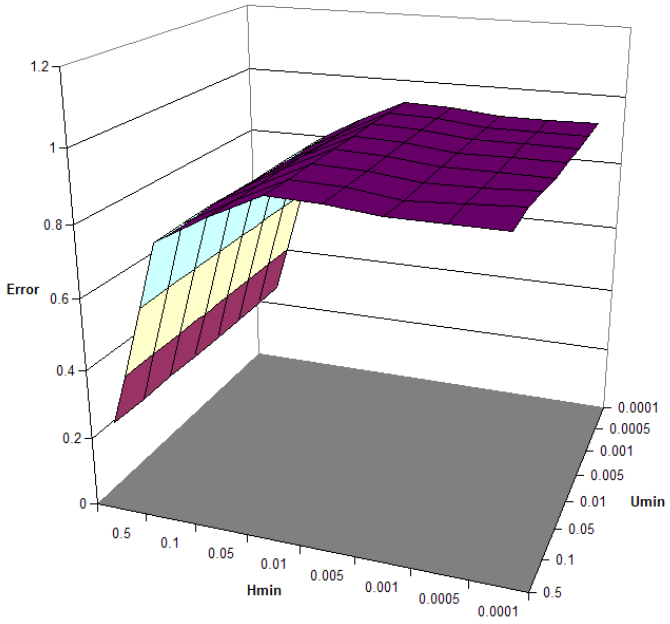

Figure 17. Mass balance errors for a range of H_{min} and U_{min} values. (See Section 2.3.) The errors on the vertical axis are shown in intervals of 200 square meters.

about 2.8 percent of the undisturbed water area for the quadratic sloping beach, while the plateau of 11 square meters in Figure 11 is about 3.1 percent of the undisturbed water area for the linear sloping beach. We believe this behavior is a function of the geometry; the wetting and drying region is shallower on the quadratic sloping beach, and thus the algorithm has less of an effect on the global water budget. Overall, however, the mass balance results are remarkably similar.

A qualitative assessment of the effect of these two parameters reveals that it is best to keep H_{min} below a reasonable limit. Figure 18 and Figure 19 show the position of the shoreline for two different combinations of H_{min} and U_{min}, each compared to a fine solution. Figure 18 shows the combination of $H_{min} = 0.01$ and $U_{min} = 0.01$, which has been used for most of the studies in this paper. It shows a reasonably good match between the coarse and fine solutions, and the coarse solution ranges from a maximum inundation of 16.25 kilometers to a maximum recession of 8.75 kilometers. Figure 19 shows the combination of $H_{min} = 0.5$ and $U_{min} = 0.01$. By increasing H_{min}, we have decreased the average mass balance error from about 900 square meters to about 250 square meters. However, we have also dramatically changed the accuracy. The match between the coarse and fine resolutions is not as good, and the maximum inundation is 15 kilometers and the maximum recession is 7.7 kilometers. The unrealistically large value of $H_{min} = 0.5$ meters allows the algorithm to dry nodes that should be wet, and it also prevents the wetting phase to extend as far up the beach. Again, without an analytical solution, there is no way to know which representation of the shoreline is correct. However, our experience with the linear sloping beach suggests that an unrealistic value for H_{min} produces unrealistic results.

Thus, results indicate an optimal value for these two parameters H_{min} and U_{min} is around 0.01. There does not appear to be a lower limit for either parameter; however, nothing is gained by decreasing either parameter to the limits of machine precision. We will continue to use values of 0.01 for both parameters in subsequent tests.

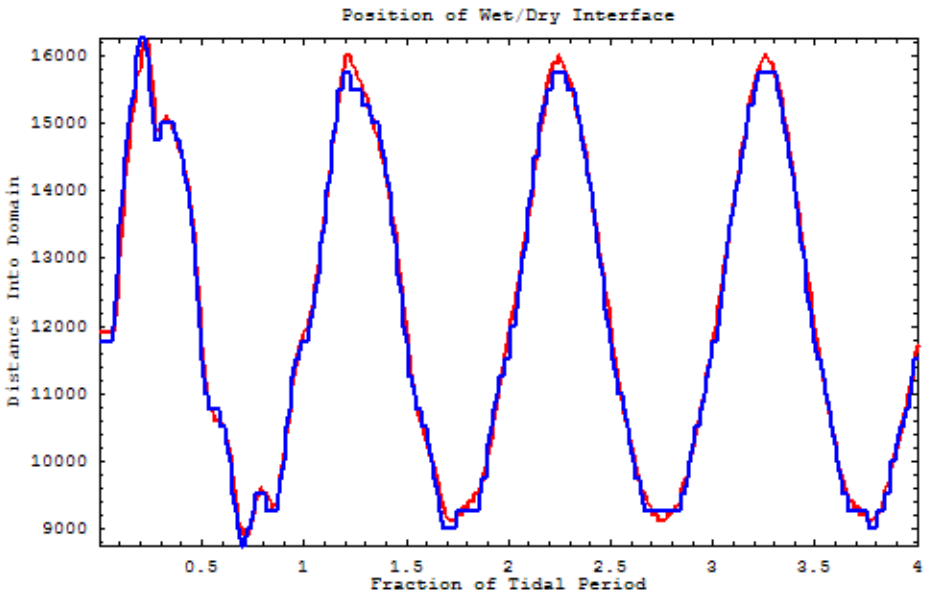

Figure 18. The position of the shoreline for the combination of $H_{min} = 0.01$ and $U_{min} = 0.01$. The blue line is a coarse solution ($\Delta x = 250$ meters, $\Delta t = 10$ seconds), and the red line is a fine solution ($\Delta x = 100$ meters, $\Delta t = 1$ second).

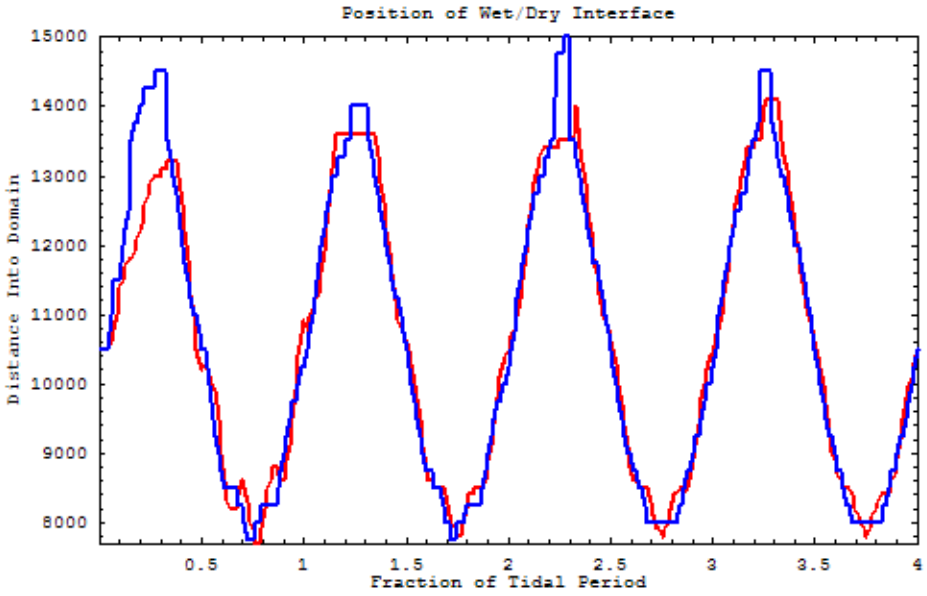

Figure 19. The position of the shoreline for the combination of $H_{min} = 0.5$ and $U_{min} = 0.01$. The blue line is a coarse solution ($\Delta x = 250$ meters, $\Delta t = 10$ seconds), and the red line is a fine solution ($\Delta x = 100$ meters, $\Delta t = 1$ second).

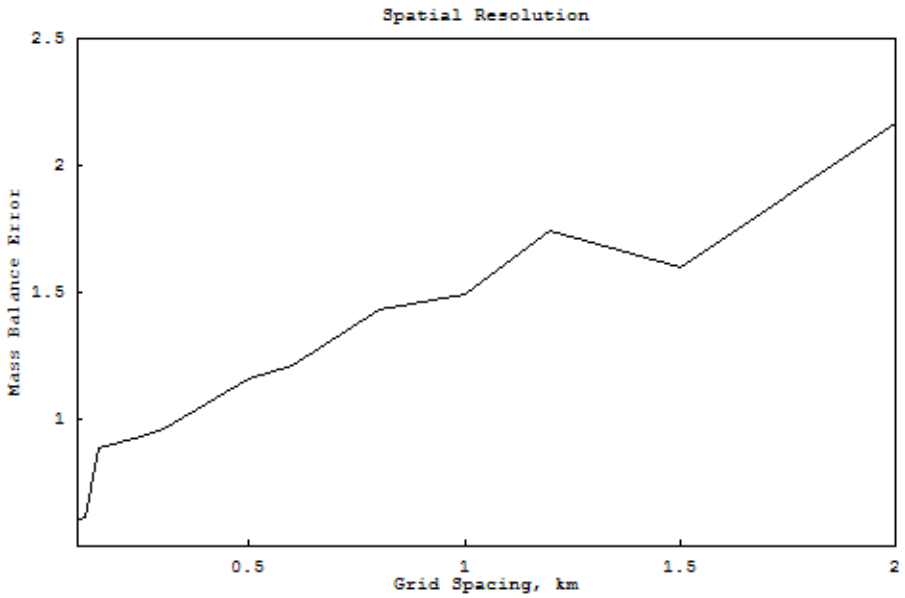

Figure 20. Mass balance errors (10^3 square meters) for a range of spatial resolutions. (See Section 2.3.)

3.2.4. Spatial Resolution

Spatial resolution also plays a significant role in the simulation of wetting and drying, because it controls the model's ability to follow the position of the shoreline as it inundates and recedes. Using the Quadratic Problem, we varied the spatial resolution from a minimum of 100 meters to a maximum of 2000 meters, where each test maintained a constant Δx. For each grid spacing, we examined the model's mass balance properties.

Figure 20 shows the mass balance errors for the various spatial resolutions. The graph shows a sublinear (0.38) convergence rate as the grid spacing is decreased. Note that all of the simulations were run with a time step of 10 seconds except for those with spatial resolutions of 100 meters and 120 meters, which were run with a time step of 1 second in order to maintain stability. This graph supports the use of the finite volume approach as a predictor of model truncation error because, as the grid spacing is decreased, the mass balance errors also decrease.

3.3. Inlet Problem

The results in this subsection are from tests on a one-dimensional slice of the Beaufort Inlet in North Carolina. First, we examine the algorithm's effect on temporal stability. Second, we conduct parameter sensitivity studies for bottom friction and the numerical G parameter. Third, we conduct parameter sensitivity studies for the wetting and drying parameters H_{min} and U_{min}. Fourth, we examine the effect of spatial resolution on the performance of the algorithm.

3.3.1. Heuristic Stability

Stability was measured by determining the maximum time step (within 5 seconds) at which the model still provided valid results. In order to prevent instabilities during the ebb phase when nodes should dry but cannot, we altered our model problem so that it can be run with the original model.

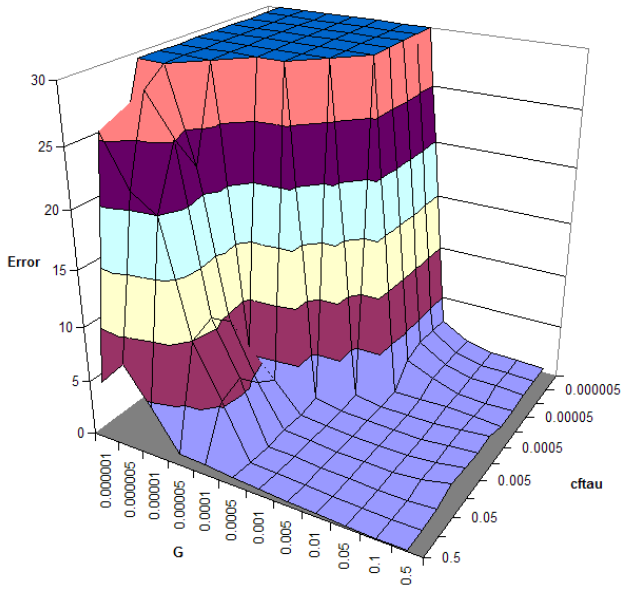

Figure 21. Mass balance errors for 144 combinations of *cftau* and *G*. The errors on the vertical axis are shown in intervals of 5,000 square meters. The errors in the region where *cftau* and *G* are near maximum are 300 square meters or less.

For the Inlet Problem, we shortened the domain to 52.8 kilometers so that there is a bathymetry of 2.5 meters at the land boundary. This prevents the 1 meter forcing amplitude from trying to dry out nodes within the inlet itself. All of the other parameters, including bathymetry, remained the same. The original ADCIRC model provided a maximum stable time step of 45 seconds. The wetting and drying model, when applied to the Inlet Problem, provided a maximum stable time step of 40 seconds, which is a decrease of 11 percent. In comparison to the previous model problems, the wetting and drying region for the Inlet Problem is a much smaller fraction of the overall domain, so the stability constraint is not as severe.

3.3.2. Parameter Sensitivity - *cftau* and *G*

The effects of the ADCIRC model parameters *cftau* and *G* on the wetting and drying algorithm were again examined. As described above in Section 3.1.3, the parameter *cftau* controls the bottom friction in the model, and the parameter *G* controls the balance between the wave continuity equation and the primitive continuity equation. Herein, we examine their effects on wetting and drying by varying the parameters from 0.000001 to 0.5 (always in sec-1 for *G*; *cftau* is dimensionless), creating a matrix of *cftau*-*G* combinations. For each combination, we examined the model's mass balance properties. Note that we were unable to compare the behavior of the model with an analytical solution, because such a solution does not exist for the Inlet Problem.

The average mass balance error for each combination is shown as a surface plot in Figure 21. The mass balance error was calculated using the finite volume approach, which is described in Section 2.3. We offer several observations. First, nearly the same region of *cftau*-*G* combinations is unstable for the Inlet Problem as had been unstable for the Quadratic Problem and the Linear Problems. The unstable region is slightly larger for the Inlet Problem, especially when *G* is

small (such as the combination of *cftau* = 0.01 and *G* = 0.000001). Second, the shape of the three-dimensional surface is similar to the shapes of the surfaces for the other problems, as shown in Figure 9 and Figure 14. However, for this problem, even the stable combinations that have a small *G* value (such as *cftau* = 0.1 and *G* = 0.000001) experience significant mass balance errors and should not be used, which was not necessarily the case for the previous two model problems. Also, for this problem, there is not as much variation in the "good" region of combinations (i.e., where *G* is at least 0.01). In this region, a slice of the matrix with a constant *G* value shows mass balance errors that are all within one order of magnitude, whereas a similar slice for the Quadratic Problem shows errors that vary over two orders of magnitude. Also, when compared to the undisturbed water area of 2.07 million square meters, these relative mass balance errors are significantly smaller. The minimum mass balance error occurs at the corner of the matrix where *cftau* = 0.5 and *G* = 0.5 and has a value of 58.8 square meters, or 0.003 percent of the undisturbed water area. The mass balance error at the combination of *cftau* = 0.0001 and *G* = 0.01 is 386.3 square meters, or 0.02 percent of the undisturbed water area. Thus, although the magnitude of mass balance errors for the Inlet Problem are similar in magnitude than the errors for the previous model problems, the larger size of the Inlet Problem diminishes their significance.

This problem is an interesting test of the wetting and drying algorithm because the minimum bathymetry occurs about three kilometers from the land boundary. In fact, this minimum bathymetry of 0.94 meters is the only place where the bathymetric depth is less than the 1.0 meter forcing amplitude. This node is located just inside the inlet opening, and, when it dries, the rest of the inlet is forced to dry as well, as described in Section 2.1. Thus, the wetting and drying processes do not occur gradually, as for the previous model problems. As the node near the inlet opening is dried, so is the rest of the inlet; and as that node is wetted, so is the rest of the inlet. Thus, the mass balance errors in the "good" region of the matrix (where $G > 0.01$) may be smaller for the Inlet Problem because the wetting and drying processes happen less often overall.

A quantitative assessment of the effect of *cftau* and *G* on accuracy could not be performed, because there is no analytical solution for the Inlet Problem. However, a review of the position of the wetting and drying interface for each combination suggests that accuracy may be significantly hindered when *cftau* is larger than 0.005. For smaller values of *cftau*, the wetting and drying processes occur four times, once for each tidal period. As *cftau* is increased above that value, the wetting and drying processes may occur only one or two times or not at all, depending on the value of *G*. This makes sense physically; as *cftau* is increased, so is the bottom friction, which would work to dampen the 1.0 meter forcing amplitude to where it would not have as much of an effect on a node that is more than 50 kilometers into the domain. Thus, users who wish to allow near-shore wetting and drying should select an appropriately small value of the bottom friction coefficient.

3.3.3. Parameter Sensitivity - H_{min} and U_{min}

The numerical parameters H_{min} and U_{min} are described above in Section 2.1, Section 3.1.4, and Section 3.2.3. Both parameters affect the ability of the algorithm to wet or dry nodes, so it is important to consider the effects of the two parameters in tandem. Each parameter was varied from 0.0001 to 0.5 (meters for H_{min}; meters per second for U_{min}), creating a matrix of combinations. For these runs, we again used *cftau* = 0.0001 and $G = 0.01$ sec^{-1}, to match the studies in Section 3.1.4 and Section 3.2.3. For each combination of H_{min} and U_{min}, we examined the model's mass balance properties.

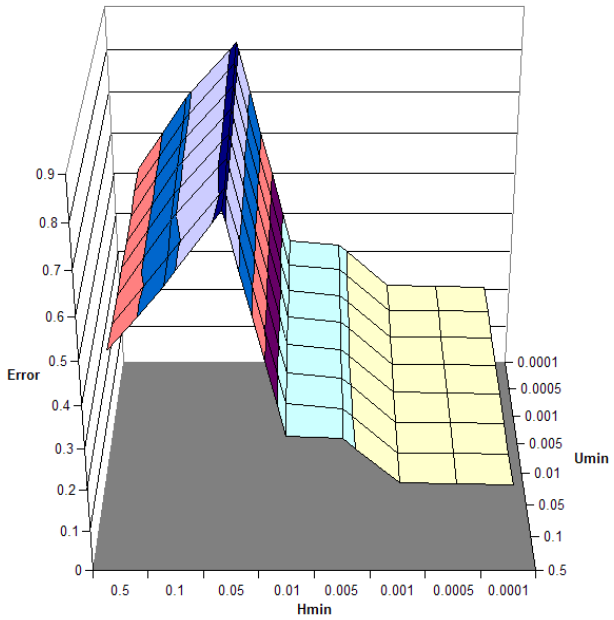

Figure 22. Mass balance errors for a range of H_{min} and U_{min} values. (See Section 2.3.) The errors are shown in intervals of 100 square meters.

The examination of the model's mass balance properties was performed in the same manner as described in Section 2.3. The mass balance error was calculated by computing the difference between the global accumulation and the global mass flux. A three-dimensional surface of average mass balance error over four tidal cycles is shown in Figure 22, and it reveals the following. First, the model does not experience instabilities for any combination of H_{min} and U_{min} within the range from 0.0001 to 0.5. Second, as with the previous two model problems, the wetting criterion U_{min} does not have an effect on mass balance. There is not a significant difference between the average mass balancer errors for the extreme values of U_{min} = 0.0001 meters per second and U_{min} = 0.5 meters per second.

Third, and most importantly, the shape of the surface is different from that of the previous two model problems. For both the Linear Problems and the Quadratic Problem, the average mass balance errors increased until about H_{min} = 0.01, and then they leveled off. For the Inlet Problem, the errors follow the same pattern until H_{min} = 0.05, but then they decrease to new minimums as H_{min} is decreased further. The unrealistically large values of H_{min} cause premature and excessive drying of the inlet region. Figure 23 and Figure 24 show the position of the wet/dry interface for two different values of H_{min}. In Figure 23, where H_{min} = 0.5 meters, the drying process occurs earlier in each tidal period than it does in Figure 24, where H_{min} = 0.0001 meters. This causes problems, especially in the first tidal period where the inlet is fully dried and wetted twice. The average mass balance errors are noticeably larger for the case when H_{min} is larger.

Thus, both the quantitative mass balance results and the qualitative accuracy results indicate that H_{min} should be kept at or below 0.01 meters at most, and there does not appear to be a penalty for decreasing it even further. Once again, the wetting criterion U_{min} does not have an effect on mass balance.

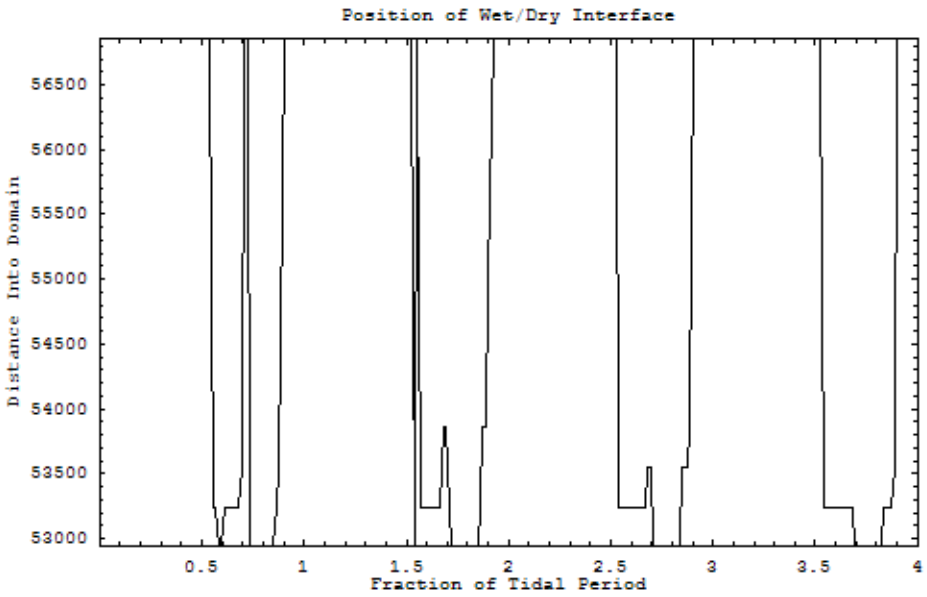

Figure 23. Position of the shoreline for the Inlet Problem. Note that H_{min} = 0.5 meters and U_{min} = 0.01 meters per second.

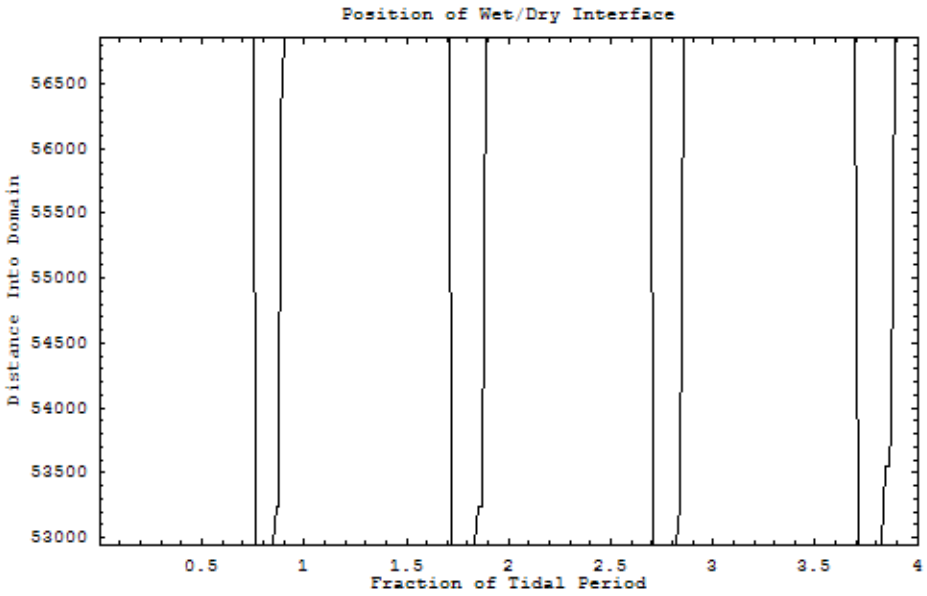

Figure 24. Position of the shoreline for the Inlet Problem. Note that H_{min} = 0.0001 meters and U_{min} = 0.01 meters per second.

3.3.4. Spatial Resolution

The effect of spatial resolution on mass balance was once again considered. Instead of using the variable spacing that is natural for the Inlet Problem, we used a constant grid spacing. Nodal bathymetries were interpolated by fitting a cubic spline to the data from the two-dimensional grid. The number of elements was varied from 25 to 400, and the corresponding spacings were varied from a maximum of about 2.3 kilometers to a minimum of 142 meters. We tried to

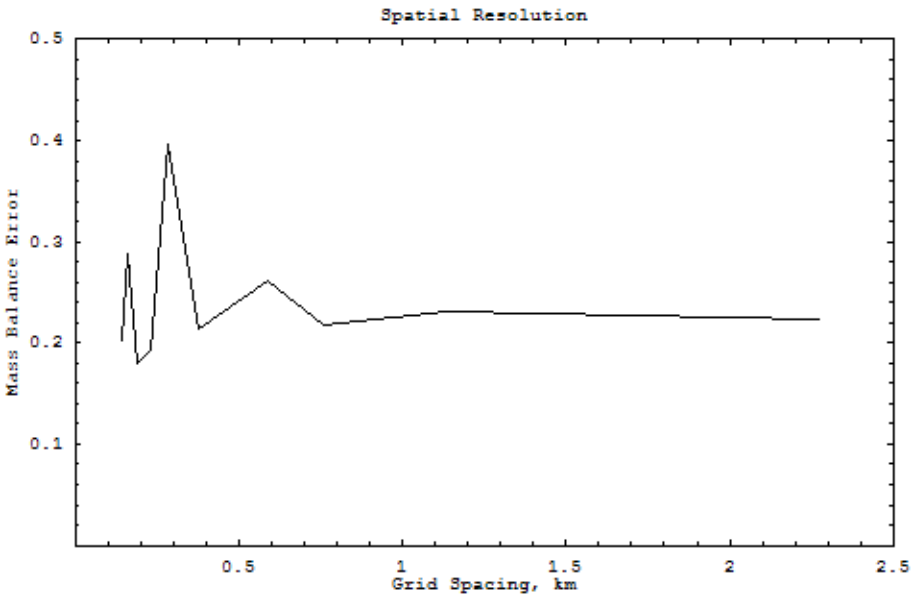

Figure 25. Mass balance errors (10^3 square meters) for a range of spatial resolutions. (See Section 2.3.)

hold the time step at a constant 10 seconds, but the fine resolutions (i.e., with 300 elements or more) required a smaller time step of 1 second.

Figure 25 shows the mass balance errors for the various spatial resolutions. Note that the mass balance errors do not converge as the grid spacing is refined. In fact, many of the smaller grid spacings produce anomalously large mass balance errors. For instance, a grid spacing of 284 meters (200 elements) produces a mass balance error of about 397 square meters. This behavior may be caused by extra wetting and drying in these simulations, as described above in Section 3.3.3. Figure 26 and Figure 27 show the position of the shoreline for two different spatial resolutions. Note that in Figure 27, where the grid spacing is smaller, there is extra wetting and drying during the second tidal cycle. The inlet is actually turned off and on twice during the same period, and this additional wetting and drying may cause the larger mass balance error.

As described in Section 2.1, the algorithm includes input parameters that can be used to prevent the rapid wetting and drying of the same node. We increased these parameters from 5 time steps to 50 time steps, but the model behavior remained the same, as shown in Figure 28. Thus, this behavior may just be start-up noise, and not a product of the algorithm itself. Note that both simulations (Figure 26 and Figure 27) fight through this start-up noise and provide similar results for the third and fourth tidal periods.

It should also be noted that all of the mass balance errors shown in Figure 25 are very small when compared to the actual size of the Inlet Problem. For instance, the maximum error of about 397 square meters is only about 0.02 percent of the undisturbed water area. Thus, although the extra wetting and drying can cause greater mass balance errors, these errors are still relatively small. Spatial resolution appears to have only a secondary effect on mass balance.

4. CONCLUSIONS

Based on the studies in this paper, we offer the following conclusions:

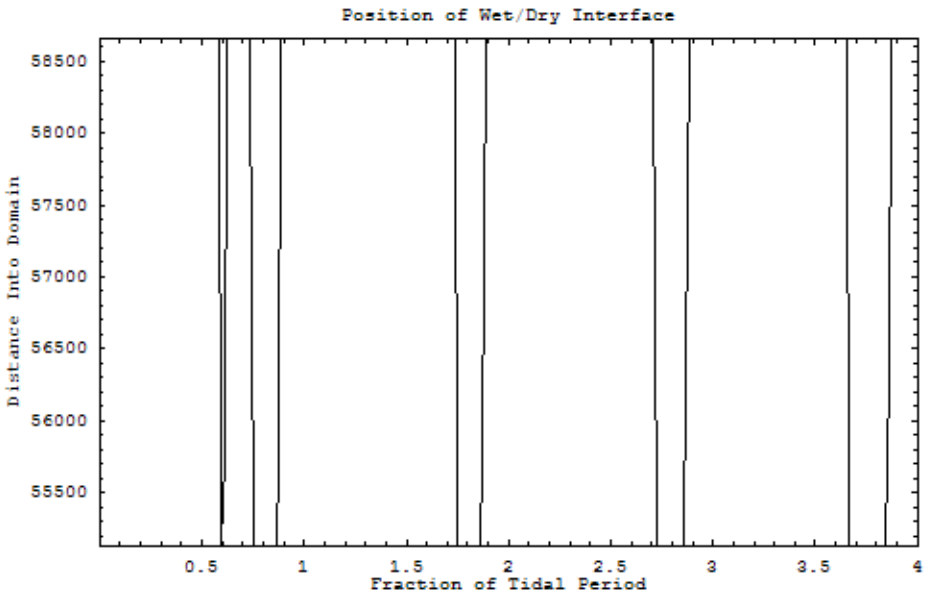

Figure 26. The position of the shoreline for the Inlet Problem. Note that the grid spacing is about 586 meters (100 elements).

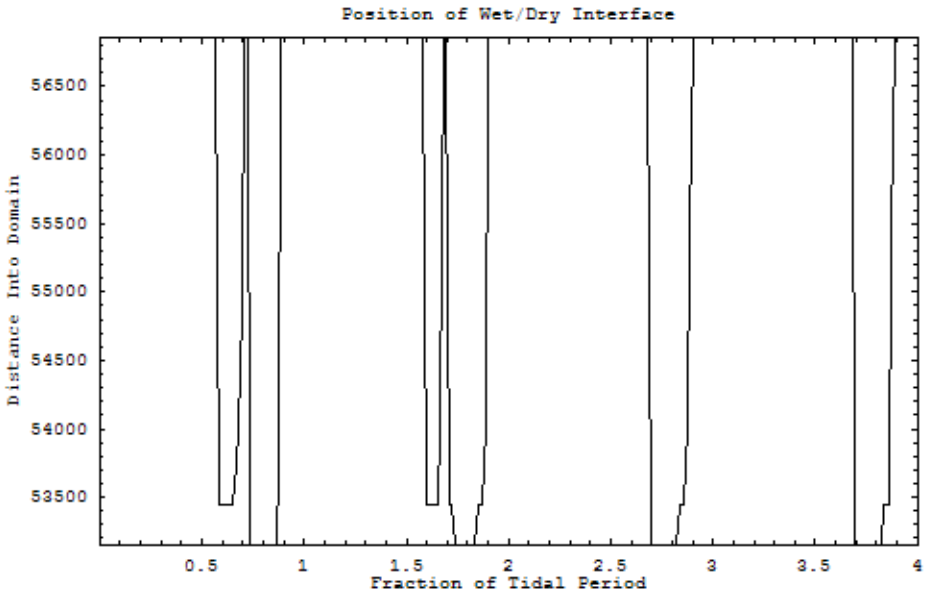

Figure 27. The position of the shoreline for the Inlet Problem. Note that the grid spacing is about 284 meters (200 elements).

- ADCIRC's wetting and drying algorithm can simulate wave run-up on beaches, even one tidal period after a cold start. Most start-up noise is concentrated in the first two tidal periods, after which the model provides better results.
- The algorithm imposes stability restrictions, which can be severe depending on the extent of the wetting and drying. Our Linear Problem 2 experienced a 70 percent reduction in the maximum stable time step, and the Quadratic Problem experienced a 66 percent reduction.

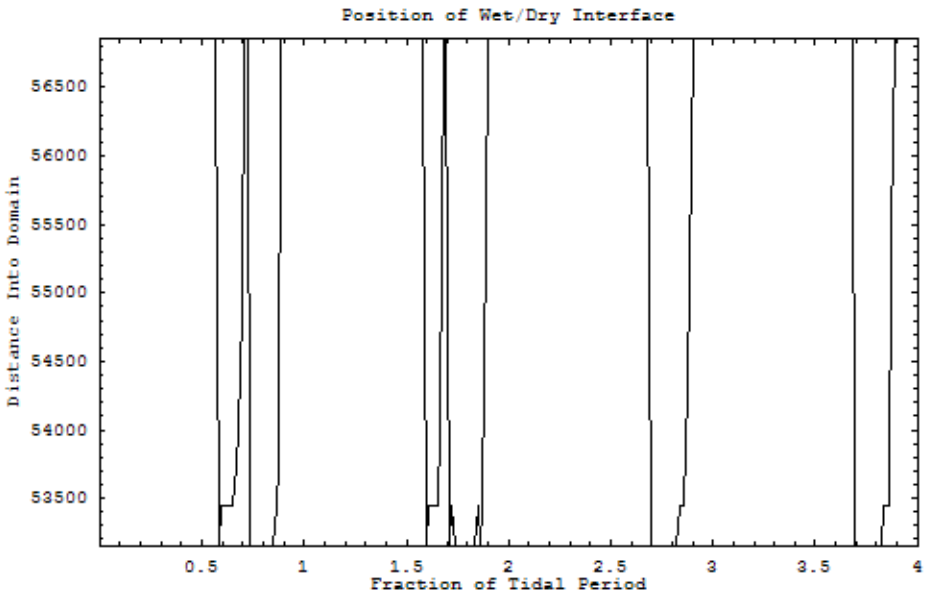

Figure 28. The position of the shoreline for the Inlet Problem. Note that the grid spacing is about 284 meters (200 elements), and that each node is required to remain dry or wet for 50 time steps before changing states.

For the Inlet Problem, where the region of wetting and drying is smaller, the decrease was 11 percent.

- The numerical parameter G must remain relatively large (i.e., greater than 0.001 sec^{-1}), especially for typical values of *cftau* in the range from 0.001 to 0.00001. However, combinations of *cftau* and G in that range show reasonable mass balance errors and values of G/τ in the same range as for non-wetting/drying barotropic applications.
- The minimum wetness height H_{min} shows acceptable behavior for all values less than or equal to 0.01 meters. Our results do not suggest that there is a lower bound for this parameter. In fact, for the Inlet Problem, mass balance errors continued to decrease as H_{min} was decreased to 0.0001 meters.
- The minimum wetting velocity U_{min} has no significant effect on the behavior of the model, for any of the four model problems.
- For the idealized model problems, accuracy and mass balance improve as the spatial resolution is refined. That trend was not evident for the Inlet Problem. However, for all four problems, a stability restriction prevents simulations with small grid spacings from being run with the same time step of 10 seconds.

5. ACKNOWLEDGEMENTS

Financial support for this research was provided, in part, by the National Science Foundation under the contract EEC-9912319, the Department of Defense under the contract ONR N00014-02-1-0651, and the University of Oklahoma. Any opinions, findings, and conclusions or recommendations expressed in this material are those of the authors and do not necessarily reflect those of the funding agencies.

REFERENCES

1. R.A. Luettich, J.J. Westerink, “An Assessment of Flooding and Drying Techniques for Use in the ADCIRC Hydrodynamic Model: Implementation and Performance in One-Dimensional Flows”, Report for the Department of the Army, Contract Number DACW39-94-M-5869 (1995).
2. R.A. Luettich, J.J. Westerink, “Implementation and Testing of Elemental Flooding and Drying in the ADCIRC Hydrodynamic Model'”, Final Report for the Department of the Army, Contract Number DACW39-94-M-5869 (1995).
3. R.L. Kolar, W.G. Gray, J.J. Westerink, R.A. Luettich, “Shallow water modeling in spherical coordinates: equation formulation, numerical implementation and application”, *Journal of Hydraulic Research*, **32(1)**, 3-24 (1994).
4. D.R. Lynch, W.G. Gray, “A wave equation model for finite element tidal computations”, *Computers and Fluids*, **7(3)**, 207-228 (1979).
5. I.P.E. Kinnmark, “The shallow water wave equations: formulations, analysis and application”, in *Lecture Notes in Engineering*, C.A. Brebbia, S.A. Orsszag (eds), Springer-Verlag, Berlin, **15**, 187 (1986).
6. R.A. Luettich, J.J. Westerink, N.W. Scheffner, “ADCIRC: an advanced three-dimensional circulation model for shelves, coasts and estuaries. Report 1: theory and methodology of ADCIRC-2DDI and ADCIRC-3DL”, Technical Report DRP-92-6, Department of the Army, USACE, Washington, DC (1992).
7. J.J. Westerink, R.A. Luettich, C.A. Blain, N.W. Scheffner, “ADCIRC: an advanced three-dimensional circulation model for shelves, coasts and estuaries. Report 2: Users Manual for ADCIRC-2DDI”, Department of the Army, USA (1994).
8. T.J.R. Hughes, G. Engel, L. Mazzei, M.G. Larson, “The continuous Galerkin method is locally conservative", *Journal of Computational Physics*, **163(2)**, 467-488 (2000).
9. R.C. Berger, S.E. Howington, “Discrete Fluxes and Mass Balance in Finite Elements”, *Journal of Hydraulic Engineering*, **128(1)**, 87-92 (2002).
10. G.F. Carrier, H.P. Greenspan, “Water waves of finite amplitude on a sloping beach”, *Journal of Fluid Mechanics*}, **4**, 97-109 (1958).
11. B. Johns, “Numerical Integration of the Shallow Water Equations over a Sloping Shelf”, *International Journal for Numerical Methods in Fluids*, **2**, 253-261 (1982).
12. G.L.D. Siden, D.R. Lynch, “Wave Equation Hydrodynamics on Deforming Elements”, *International Journal for Numerical Methods in Fluids*, **8**, 1071-1093 (1988).
13. R.L. Kolar, J.J. Westerink, M.E. Cantekin, C.A. Blain, “Aspects of Nonlinear Simulations using Shallow-Water Models based on the Wave Continuity Equation”, *Computers and Fluids*, **23**, 523-538 (1994).
14. R.A. Luettich et al, “Barotropic Tidal and Wind Driven Larvae Transport in the Vicinity of a Barrier Island Inlet”, *Journal of Fisheries Oceanography*, **8**, 190-209 (1999).